

Evaluation of the Met Office global forecast model using Geostationary Earth Radiation Budget (GERB) data

By R. P. ALLAN^{1*}, A. SLINGO¹, S. F. MILTON² and M. E. BROOKS²

¹University of Reading, UK

²Met Office, UK

(DRAFT 1, 12th December 2006)

SUMMARY

Simulations of the top of atmosphere radiative energy budget from the Met Office global Numerical Weather Prediction (NWP) model are evaluated using new data from the Geostationary Earth Radiation Budget (GERB) instrument on-board the Meteosat-8 satellite. Systematic discrepancies between the model simulations and GERB measurements greater than 20 Wm^{-2} in outgoing longwave radiation (OLR) and more than 60 Wm^{-2} in reflected shortwave radiation (RSW) are identified over the period April–September 2006 using 12 UTC data. A positive model OLR bias greater than 30 Wm^{-2} over the west Sahara during July is found to be present for clear-sky conditions and consistent with high aerosol optical depth from independent satellite measurements, consistent with previous findings. Convective cloud over equatorial Africa is spatially less organised and less reflective than in the GERB data. This bias is highly sensitive to changes in the model convective parametrization. Over the same region, the observed diurnal variation of OLR is captured by the model although afternoon OLR is lower in the satellite data; this is consistent with a later peak in diagnosed convective cloud in the model compared to the satellite data. Underestimates in model OLR over the Gulf of Guinea coincide with unrealistic southerly cloud outflow from convective centres to the north. Finally, large overestimates in model RSW over the ocean, greater than 50 Wm^{-2} at 12 UTC, are related to unrealistic radiative properties of marine stratocumulus cloud. The results of this analysis contribute to the development and improvement of parameterisations in the global forecast model.

KEYWORDS: Radiative processes Numerical Weather Prediction Cloud

1. INTRODUCTION

- Tony to write this if he would like! Very basic intro below...

Simulations of the top of atmosphere radiation budget from the Met Office global Numerical Weather Prediction (NWP) model have been routinely compared with observations from the Geostationary Earth Radiation Budget (GERB) instrument (Harries *et al.* 2005) since May 2003 (Allan *et al.* 2005). As well as contributing to data validation (Harries *et al.* 2005; Allan *et al.* 2005), the methodology has been successfully applied in the examination of radiative processes (Haywood *et al.* 2005; Comer *et al.* 2007) and in model evaluation and development (Milton *et al.* 2005; Allan *et al.* 2006). In the present study, we update previous analysis by using the release version GERB data to evaluate the current version of the NWP model over the period April–September 2006.

2. MODEL AND DATA DESCRIPTION

(a) Global forecast model

- Sean to write brief description.

·
·
·

* Corresponding author: Environmental Systems Science Centre, University of Reading, Reading, Berkshire, RG6 6AL, UK

© Royal Meteorological Society, 2002.

- Refer to description of model and methodology in Allan *et al.* (2005)
- describe important updates to model (e.g. 17 Aug 2005 soil moisture, 20th Dec 2005 improved resolution, 14th March 2006, improvements to convection and boundary layer).

(b) *Satellite and ancillary data*

Edition 1 ARG (Averaged, Rectified, Geolocated) level 2 broad-band radiative flux data from the Geostationary Earth Radiation Budget (GERB; Harries *et al.* 2005) instrument are considered in detail for the period April-September 2006. The absolute accuracy is estimated at 2.25% for solar radiance and 0.96% for thermal radiance. Broad-band radiative fluxes are derived from the unfiltered measured radiance using angular dependence models which are likely to incur additional uncertainty of order 5 Wm^{-2} for thermal fluxes and 10 Wm^{-2} for typical solar fluxes (Slingo *et al.* 2006). Higher errors may be present for aerosol and high, thin cloud (Jacqui Russell pers. comm.). The temporal resolution is approximately 17 minutes. Here we use the time-slots closest to the model 15-minute time-steps commencing every 3-hours from 00 UTC.

In addition to the flux products, a cloud fraction product, generated as part of the GERB processing is used in the analysis. This was developed by the Royal Meteorological Institute of Belgium (RMIB) by Ipe *et al.* (2004) based on shortwave channels from the Spinning Enhanced Visible and InfraRed Imager (SEVIRI) also on-board the Meteosat-8 satellite (Schmetz *et al.* 2002). Also based on SEVIRI data is the Meteorological Product Extraction Facility (MPEF) cloud mask which is available night and day.

We also utilise $0.55\mu\text{m}$ aerosol optical depth data from the Multi-angle Imaging Spectroradiometer (MISR Version AM1_CGAS_F06_0021; Diner *et al.* 2001), Cloud Liquid Water (CLW) data from the Special Sensor Microwave Imager (SSM/I, Version 6; Wentz 1997) and vertical velocity fields from the National Centers for Environmental Prediction/National Center for Atmospheric Research (NCEP/NCAR) 40-year reanalysis (Kalnay *et al.* 1996).

(c) *Methodology and Definitions*

We use the methodology described in Allan *et al.* (2005) to generate model fluxes and additional diagnostics at the model analysis times (commencing at 00, 06, 12, 18 UTC) for the model time-step duration of 20 minutes. Additionally, 3-hour forecasts run from the model analysis times are used to generate a further 4 sets of 20 minute time-steps at (03, 09, 15, 21 UTC) for some of the period considered. A 3-hour frequency archive of model and GERB/SEVIRI comparisons are subsequently generated. The GERB and model data are interpolated onto a regular grid of resolution 0.833° longitude by 0.556° latitude. This is the resolution of the NWP model prior to December 2005 whereupon the model resolution was increased to 0.5625° longitude by 0.375° latitude. Unless stated, all analysis is conducted using the lower-resolution interpolated model data. This ensures that both the model and GERB data undergo an interpolation step in the processing as well as allowing backward compatibility with an earlier version of the NWP model.

The outgoing longwave radiation (OLR) and reflected shortwave radiation (RSW) at the top of the atmosphere are simulated by the model and compared with the corresponding quantities from GERB. Additionally, the incoming solar

radiation (ISW) at the top of the atmosphere is calculated, in a consistent manner to the model parametrisation, for the exact time of the GERB RSW observations as described in Allan *et al.* (2005). This helps in the reduction of differences in RSW due to the temporal mis-match between the GERB and model time-steps

Cloud fraction (Ac) is an additional diagnostic generated by the model and in the processing of the GERB data (RMIB) and SEVIRI data (MPEF); these are used to generate consistently sampled clear-sky (Type I) diagnostics from the model and GERB in addition to the clear-sky fluxes generated within the model by setting cloud fraction to zero (Type II) as described in Allan *et al.* (2005).

Additional diagnostics are calculated from the model and GERB top of atmosphere radiative fluxes. Shortwave albedo (α) is calculated as the fraction of ISW that is reflected back to space as RSW. The longwave cloud radiative effect (LWCF) is calculated as,

$$LWCF_{gerb} = OLRc_{model} - OLR_{gerb}, \quad (1)$$

$$LWCF_{model} = OLRc_{model} - OLR_{model}, \quad (2)$$

where $OLRc_{model}$ is the model simulated clear-sky OLR. The albedo cloud forcing (ALBCF) is calculated as,

$$ALBCF_{gerb} = \alpha_{gerb} - \alpha_{c,model}, \quad (3)$$

$$ALBCF_{model} = \alpha_{model} - \alpha_{c,model}, \quad (4)$$

where $\alpha_{c,model}$ is the model simulated clear-sky albedo. The analysis of Allan *et al.* (2005) suggested that simulated clear-sky fluxes over the ocean agreed with coincident preliminary GERB data to within ± 5 - 10 Wm^{-2} for OLRc and ± 0.01 for shortwave albedo. The GERB calculated LWCF and ALBCF are also limited by these errors.

3. GLOBAL COMPARISON FOR 12 UTC DATA

Composites of the consistently sampled model minus GERB differences in OLR and RSW over the period April-September 2006 were generated using 12 UTC data (Fig. 1). Also shown are the clear-sky composites using only pixels for which both the model and satellite data indicated cloud cover below 1%.

Differences in OLR over much of the oceans are generally within about 5 Wm^{-2} suggesting that systematic model errors in mean temperature and humidity and upper-level clouds are relatively small. Larger differences occur at the southern and eastern limb; this is likely to relate to increased uncertainty in the GERB data. A slight positive model OLR bias of order 10 Wm^{-2} over parts of the sub-tropical and mid-latitude Atlantic is also present when only sampling clear-sky scenes.

There are model minus GERB differences substantially greater than the expected uncertainty in the satellite data. Over Europe, the model overestimates OLR by 10 - 20 Wm^{-2} and underestimates RSW by over 50 Wm^{-2} . This signal is not present in the clear-sky cases or at other model analysis times and is consistent with an underestimation in simulated cloud cover at midday. The north African region is characterised by overestimates in Saharan OLR and underestimates in RSW over the sub-Saharan regions including the Sahel and northern coast of Africa. These signals originate from the clear-sky scenes and in the case of the longwave radiation are present also for 18 UTC but less so at 06 UTC.

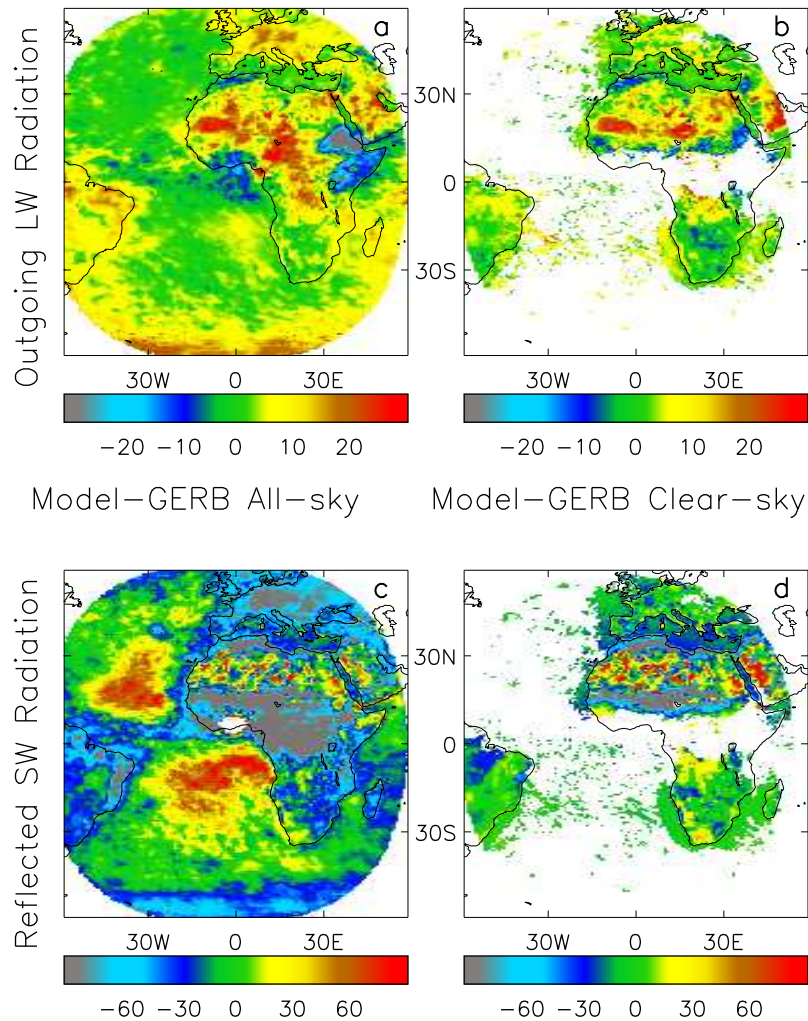


Figure 1. Model minus GERB (a) OLR, (b) clear-sky OLR, (c) RSW and (d) clear-sky RSW at 1200 UTC for the period April-September 2006.

Over the tropics the model underestimates OLR over the Ethiopian highlands and the Gulf of Guinea while overestimating OLR in the region of the Cameroon Highlands. These anomalies are not apparent in the clear-sky or shortwave comparisons suggesting that they relate to errors in upper-level cloud properties. Considering other model analysis times (not shown) the signals are also present, peaking over the Ethiopia highlands at 12 UTC, Cameroon at 18 UTC and the Gulf of Guinea at 0-6 UTC. It is not clear whether these anomalies are linked although the tri-pole pattern and timings are indicative of a coupling. A substantial underestimation of model RSW ($\sim 100 \text{ Wm}^{-2}$) is apparent over tropical convective regions of Africa while the model overestimates RSW over the marine stratocumulus regions of the Atlantic up to a similar magnitude.

Time series of mean OLR and shortwave albedo over the GERB-field of view at 12 UTC and the model minus GERB differences are shown for ocean (Fig. 2) and land (Fig. 3) regions. This includes the preliminary pre-release GERB data in

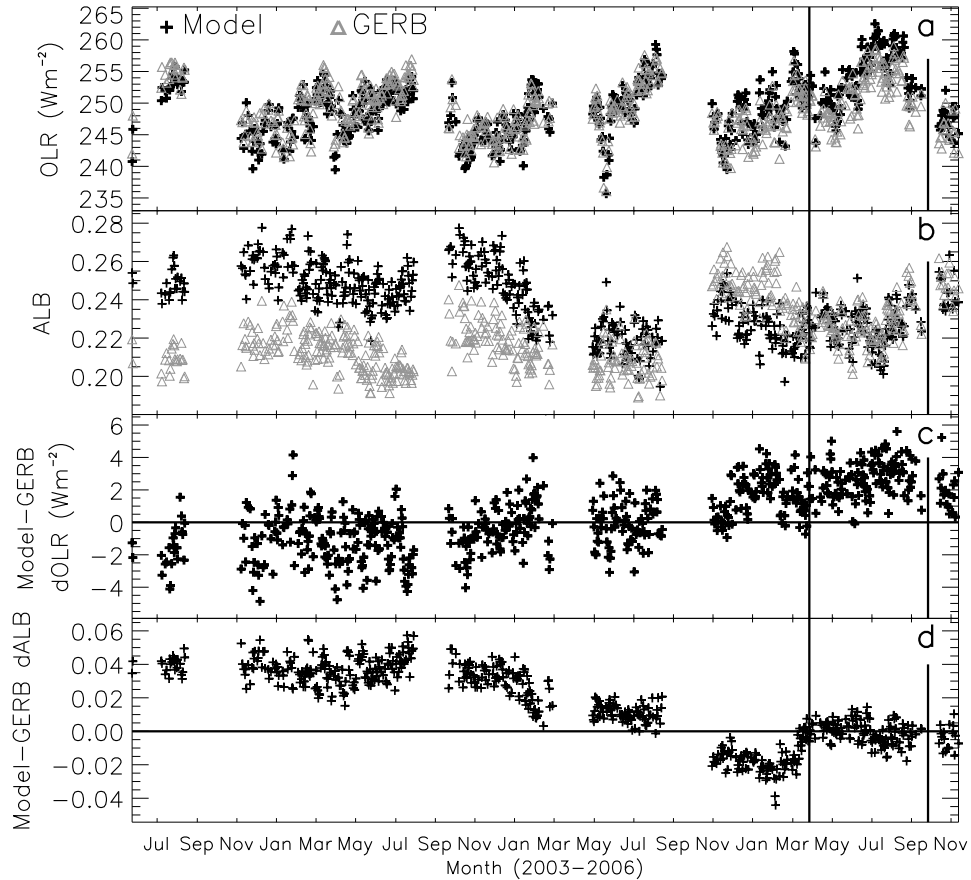


Figure 2. Time series of global ocean averages over the GERB-field of view for (a) OLR, (b) albedo and model minus GERB (c) OLR difference and (d) albedo differences. The period April-September 2006 contains the Edition 1 GERB data (denoted by vertical lines); other GERB data are pre-release versions and are unvalidated.

addition to the April-September Edition 1 GERB data for comparison purposes only.

The observed daily and seasonal variability in OLR is well captured by the model with agreement to within about 5 Wm^{-2} (Fig. 2a). The period of Edition 1 GERB data exhibits a positive model minus GERB differences (Fig. 2c); considering Fig. 1a, this originates in part from the southern and eastern satellite viewing limb where the GERB data is most uncertain, but also from other areas such as the south Atlantic marine stratocumulus region. The mean bias, of about 3 Wm^{-2} , is similar to the absolute GERB accuracy of 1%.

Variation in shortwave albedo in Fig. 2c and d shows large discrepancies, in particular for 2003-04. This in part relates to changes in the processing of the preliminary GERB data but also to changes in model parametrizations. The April-September 2006 period shows excellent agreement between GERB and the model in the mean although there exist compensating errors over the marine stratocumulus regions (positive model minus GERB differences) and the Inter tropical Convergence Zone (ITCZ) and south-eastern limb (negative differences) as shown in Fig. 1c. The increase in model albedo before the April-September

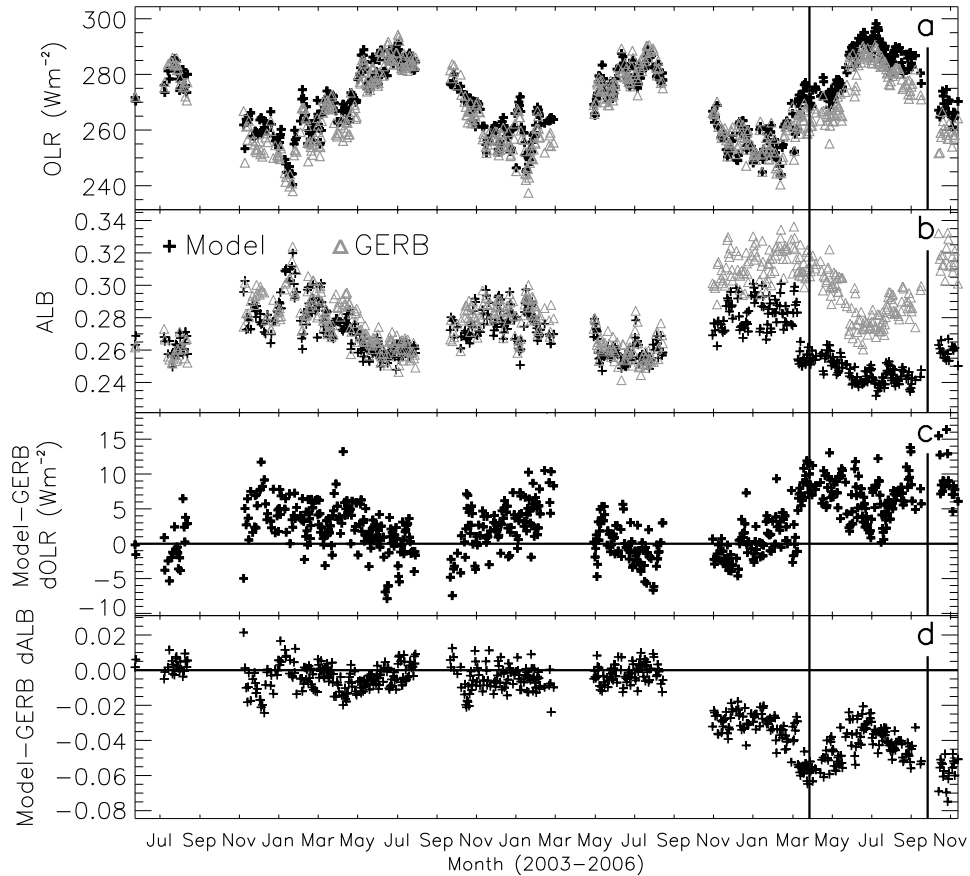


Figure 3. Time series of global land averages over the GERB-field of view for (a) OLR, (b) albedo and model minus GERB (c) OLR difference and (d) albedo differences. The period April-September 2006 contains the Edition 1 GERB data (denoted by vertical lines); other GERB data are pre-release versions and are unvalidated.

2006 period originates from the 14th March 2006 and relates to changes in the boundary layer and convective parametrizations implemented in the model at this time (Allan *et al.* 2006).

For land regions, OLR variation is larger over the seasonal cycle (Fig. 3a) mainly due to the heating and cooling of the northern hemisphere land masses. As for ocean regions, the model simulates these variations well but with a larger positive model minus GERB bias of around $5-10 Wm^{-2}$ for the April-September 2006 period. This positive bias originates from a variety of regions including equatorial Africa and Europe but also for the predominantly clear-sky north Africa-Saudi Arabian regions.

In contrast to the ocean comparisons, the April-September 2006 period displays much larger bias in shortwave albedo compared to the earlier part of the time period with a relatively small mean discrepancy before September 2005. The larger GERB albedo after September 2005 coincide with a major change in the GERB processing including a modified spectral response. However, a big drop in model shortwave albedo is also evident in March 2005, relating to the changes in parametrizations, in particular a decreased convective cloud albedo over tropical

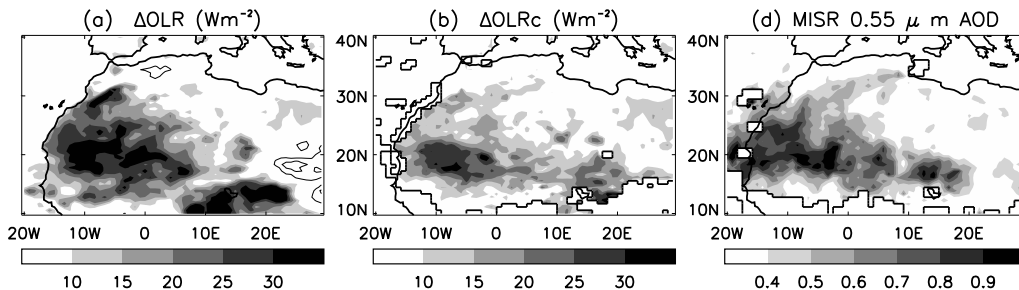


Figure 4. Mean model minus GERB (a) OLR and (b) clear-sky OLR for 12, 15 and 18 UTC data and MISR monthly mean aerosol optical depth at $0.55\mu\text{m}$ for July 2006. In (a) contours are also placed at -10 and -20 Wm^{-2} ; missing data regions in (b) and (c) are represented by the blocked contour.

Africa relating to the implementation of modified adaptive detrainment in the convection parametrisation (##Model paper. REF?; Allan *et al.* 2006). This is clearly evident in Fig. 1c which shows large negative model minus GERB differences in RSW over tropical Africa. Also contributing to the area-mean bias for this period are overestimations in RSW over Europe for cloudy scenes and over the Sahel and north African coastal countries for clear-sky scenes.

We now analyse in more detail the main discrepancies between model and GERB data and relate this to radiative processes including mineral dust aerosol effects over the Sahara, convection over equatorial Africa, convectively generated cloud over the Gulf of Guinea and marine stratocumulus cloud over the south Atlantic.

4. REGIONAL STUDIES

(a) Mineral Dust Aerosol over the Sahara

The largest model minus GERB OLR differences at 12 UTC are found over northern Africa (Fig. 1a). A large proportion of the positive bias remains when sampling only coinciding clear-sky scenes with differences reaching about 30 Wm^{-2} . Previously, Haywood *et al.* (2005) identified a comparable signal when comparing a previous version of the NWP model with Meteosat-7 data in July 2003 and used detailed radiative transfer calculations to argue that mineral dust aerosol was the most likely cause of the discrepancy.

Analysing time series of model minus GERB OLR differences over the western Sahara region (not shown), it is apparent that positive differences greater than 20 Wm^{-2} are most common during the period May-August. For comparison with Haywood *et al.* (2005), model minus GERB OLR differences are presented in Fig. 4a but using 12, 15 and 18 UTC data from July 2006. The discrepancy is similar in structure to that found using 12 UTC data from April-September in Fig. 1b but of a larger magnitude. Negative model minus GERB OLR differences are denoted by contours; these are smaller in magnitude than the positive (shaded) differences. The discrepancy is consistent with the findings of Haywood *et al.* (2005) for July 2003.

To remove the effects of cloud, which can induce both positive and negative bias in model OLR, the data in Fig. 4a was sub-sampled, retaining only pixels in which both model and satellite data contain less than 5% cloud cover (Fig. 4b). The difference magnitude is diminished slightly relative to Fig. 4a, although

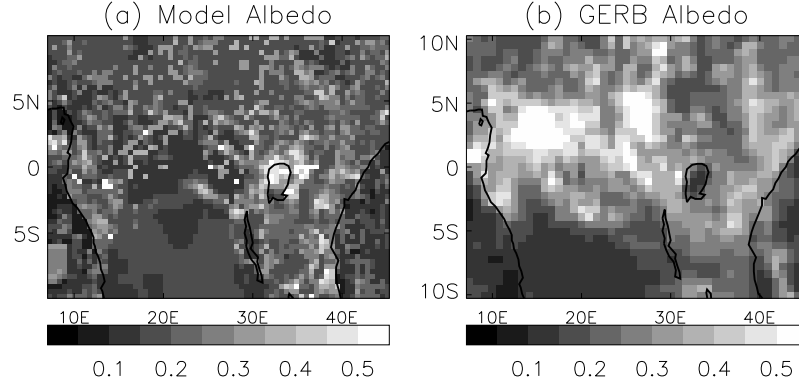


Figure 5. Shortwave albedo at 1200 UTC, 5th June 2006 over equatorial Africa for (a) high resolution model data and (b) GERB

differences of up to 30 Wm^{-2} remain across the western Sahara. The spatial pattern of the clear-sky OLR differences is well correlated (correlation coefficient of 0.66) with high monthly mean aerosol optical depth at $0.55 \mu\text{m}$ measured by the MISR instrument (Fig. 4c) and with TOMS daily aerosol index (not shown), supporting the findings of Haywood *et al.* (2005) that the exclusion of mineral dust aerosol in the global NWP model seriously compromises the longwave radiative energy balance of the model.

Using ground-based instruments and satellite data, including GERB, Slingo *et al.* 2006 identified large perturbations to the shortwave and longwave column radiative divergence relating to a dust storm in March 2006. Work is currently underway to assess the model simulations over this region (## Sean REF##). Since the atmospheric radiative cooling rates exert a crucial forcing on the large-scale dynamics, it is important to assess the practicalities of including mineral dust aerosol schemes of various sophistication in climate and NWP models (##REF: Jim Haywood##).

(b) Convection across Equatorial Africa

Large differences in OLR of order 30 Wm^{-2} and in RSW greater in magnitude than 90 Wm^{-2} were identified over equatorial Africa using 12 UTC data from April-September 2006 (Fig. 1). In this section we concentrate on the large underestimation in model shortwave albedo over continental Africa land within 10° of the equator.

Figure 5 shows instantaneous model and GERB shortwave albedo field for 12 UTC on the 5th June 2006. Here we use the original (uninterpolated) model resolution to highlight the structure of convection. The general region of high albedo, symptomatic of deep convective cloud, is similar in the model and GERB data. For example, the dark, cloud-free regions observed to the north-west and, more especially, south west of the region are captured by the model. However, consistent with previous analysis (e.g. Allan *et al.* 2005) the spatial structure of convective cloud appears more organised in the satellite data compared to the scattered, pixelised model albedo field. Also apparent is the underestimation of albedo in the cloudy regions; apparently cloudy model pixels commonly indicate $\alpha \sim 0.3$ while the main convective centres in the GERB data contain shortwave albedo greater than 0.5.

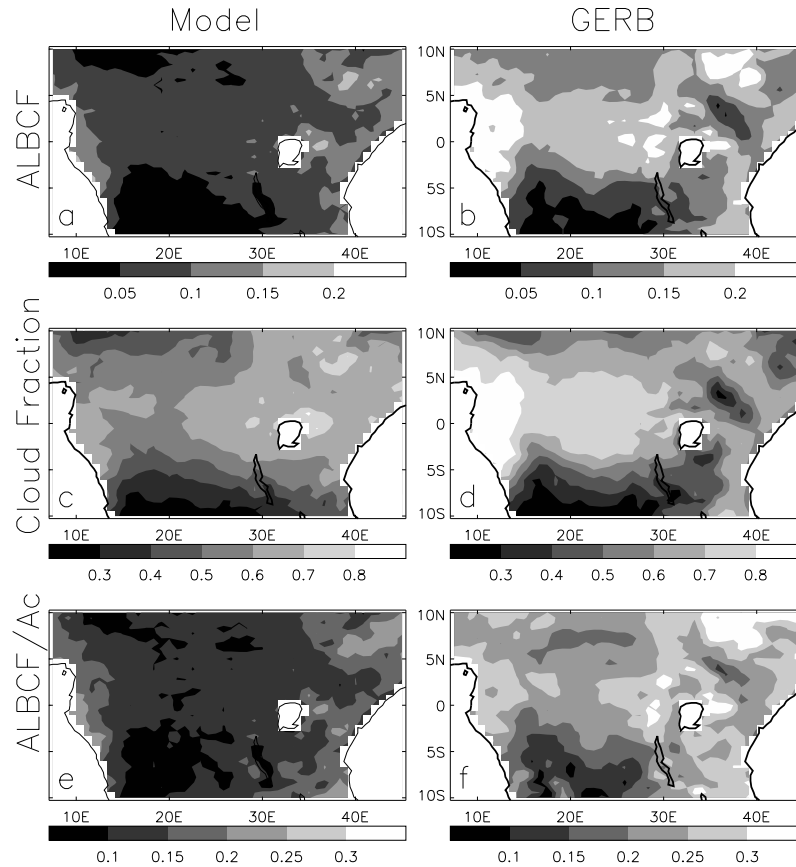


Figure 6. Shortwave albedo at 1200 UTC (April-September 2006), over equatorial Africa: albedo cloud forcing for (a) model and (b) GERB; cloud fraction for (c) model and (d) Meteosat-8 and cloud albedo forcing normalised by cloud fraction for (e) the model and (f) GERB.

The underestimation in cloud albedo is also apparent for the global land time series in Fig. 3b from April 2006 onwards. A drop in model albedo is also apparent during March 2006 which coincided with changes in convective parametrisation on 14th March; this change in model albedo is most pronounced over tropical Africa (not shown).

One possible explanation for the model underestimation in shortwave albedo is an underestimation in cloud cover. Figure 6 shows the model and GERB albedo cloud forcing (ALBCF), calculated as the difference between albedo and model clear-sky albedo, and cloud fraction for the period April-September 2006. The model substantially underestimates the mean albedo over equatorial Africa with values around 0.1 compared with the GERB values of 0.15 to 0.2. There is evidence that the model also underestimates cloud fraction over western equatorial Africa which helps to explain the some of the discrepancy in albedo. However, differences in cloud fraction are smaller over eastern equatorial Africa and when albedo cloud forcing is normalised by cloud fraction, which essentially removes the effect of cloud fraction on the albedo differences, a negative bias remains in the model data compared with GERB/Meteosat-8. Therefore the

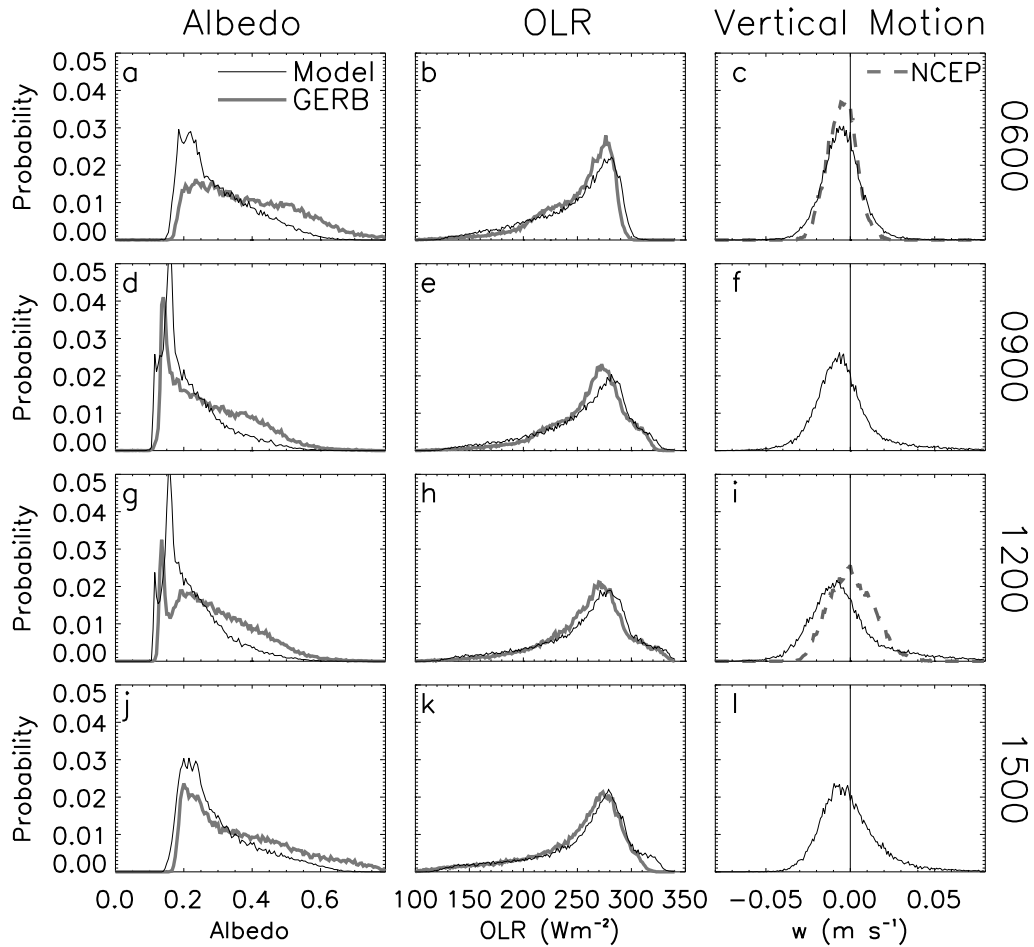


Figure 7. Probability histograms for shortwave albedo, OLR and 500 *mb* vertical motion at 06 UTC (a-c), 09 UTC (d-f), 12 UTC (g-i) and 18 UTC (j-l) for model and GERB data. NCEP vertical motion probability histograms are also shown for (c) 06 UTC and (i) 12 UTC.

most likely cause of the model underestimation in RSW over tropical Africa is unrealistically low reflection from deep convective cloud.

To understand more fully the nature of the cloud radiative errors we now analyse histograms of OLR and albedo fields along with vertical motion diagnostics for 06, 09, 12 and 15 UTC. Fig. 7. It is apparent that the model underestimates the high albedo ($\alpha > 0.4$) probabilities for all times considered. While the very lowest albedo probability distribution appears reasonably consistent between the model and GERB, symptomatic of the clear regions, the model overestimates the probability of albedo around 0.2.

Histograms of OLR probability are in much better agreement compared to albedo indicating that the cloud height and clear-sky atmosphere are well simulated by the model. However, the probability of simulated OLR greater than 300 Wm^{-2} , corresponding to clear-sky, are overestimated compared with GERB at 15 UTC.

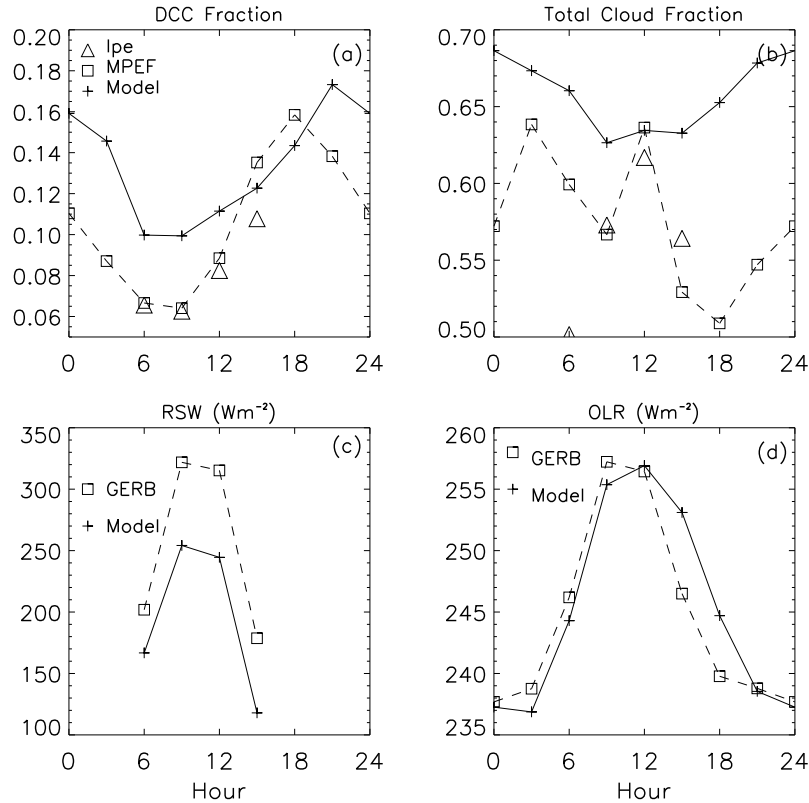


Figure 8. July 2006 average diurnal cycle in (a) high cloud, (b) total cloud, (c) reflected shortwave radiation and (d) OLR over equatorial Africa.

Vertical motion histograms peak at below zero indicating the predominance of downward motion, even for this convectively active region. However, for 09, 12 and 15 UTC, there is a long tail in the distribution for positive (upward) velocities, symptomatic of deep convection. While the model vertical velocity distribution is similar to the NCEP data for 06 UTC, the peak probability at negative velocities and the long tail for positive velocities is not present in the NCEP data for 12 UTC. This may be a deficiency in NCEP data; Trenberth and Guillemot (1998) also noticed the lack of strong vertical velocities in the NCEP data. Nevertheless, the histograms of radiation and dynamical diagnostics suggest systematic differences with GERB and NCEP data, some of which are sensitive to the time of day.

The diurnal cycle of tropical convection has long been a problem for general circulation models (e.g. Slingo *et al.* 2004) and we now consider changes over equatorial Africa for the July mean diurnal cycle at a frequency of 3-hours (Fig. 8). To identify deep convective cloud the following criteria is applied:

$$\frac{LWCF}{Ac} > 80Wm^{-2}; Ac > 0.9. \quad (5)$$

This ensures that high-altitude, thick cloud is sampled consistently in the model and GERB data; thick cirrus anvils may also be included in this identification as well as deep convective cloud.

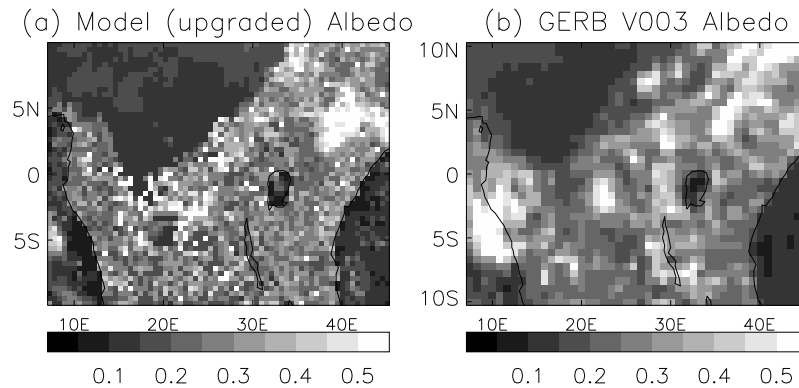


Figure 9. Shortwave albedo at 1200 UTC, 5th December 2006 over equatorial Africa for (a) high resolution model data (upgraded with new parametrizations) and (b) GERB V003 pre-release version data

The 3-hour frequency convective cloud, identified in the model, MPEF and RMIB cloud diagnostics, are presented in Fig. 8a. The RMIB cloud product is only available for 06 to 15 UTC time slots; there is good agreement between MPEF and RMIB although RMIB is lower for 15 UTC, partly due to missing data in the east where solar zenith angle is low. Apart from at 15 and 18 UTC, the model slightly overestimates convective cloud fraction. The MPEF diagnosed convective cloud fraction peaks at 18 UTC, 3-hours before the model peak. A general overestimation in model total cloud fraction is also apparent (Fig. 8b). This bias is of the opposite sign to explain the lower RSW in the model compared to GERB (Fig. 8c). Note that the anomalously low RMIB total cloud fraction at 06 UTC is influenced by missing data and higher uncertainty at the low sun angles. Interestingly, the MPEF total cloud fraction minimum coincides with the peak in diagnosed convective cloud while the model total and convective cloud fractions are in phase to within about 3-hours.

Despite the large cloud fractions in this convectively active region, the diurnal changes in OLR are strongly affected by solar heating of the land (Comer *et al.* 2007) as highlighted by the peak close to 12 UTC in both the model and GERB data (Fig. 8d). The model captures the diurnal cycle in GERB OLR despite the apparent overestimation of total and convective cloud fraction compared to RMIB and MPEF. At 15 and 18 UTC, where model and observed convective cloud fraction agree to within 0.01, the model overestimates OLR compared to GERB. Considering the OLR histogram at 15 UTC (Fig. 7k), it is likely that the higher model OLR originates from the clear-regions (highest OLR values), far from the convective centres.

The model underestimation in RSW over equatorial Africa over the period April-September, appears unrelated to biases in cloud fraction and was related to an update in the model parametrizations on the 13th March 2006 relating to convective clouds. Nevertheless, even before this model update, the spatial structure and reflectivity of convective cloud was prone to large errors (Milton *et al.* 2005; Allan *et al.* 2006). Part of the problem arises from the unrealistic intermittency of convection and Convective Available Potential Energy (CAPE) closure adjustment time-scales (Milton *et al.* 2005). To alleviate the problem of intermittency of convection, a decay time-scale was introduced into the model

convection parametrisation on 5 December 2005 (##REF?). Fig. 9 illustrates the improvement in model simulation of the top of atmosphere shortwave albedo over the equatorial African region compared to preliminary GERB data relative to the earlier comparison in Fig. 5.

(c) *Convectively Generated Cloud over the Gulf of Guinea*

A negative model OLR bias over the Gulf of Guinea (Fig. 1a) coincides with a region of active convection and cirrus cloud (Comer *et al.* 2007). Analysing the model data in more detail it is also apparent that higher altitude cloud, inferred from its strong effect on OLR and relatively weaker effect on shortwave albedo at mid-day, is often present. Detailed comparisons of model and GERB OLR over the Gulf of Guinea are now conducted using 3-hourly data during July 2006.

Figure 10a-b shows the time-latitude evolution of OLR (shading) for the model and GERB. Overlaid are contours of MPEF cloud fraction at 40% and 80%, smoothed over 12 hours for clarity. In general the model overestimates cloud fraction compared with MPEF which is consistent with the negative OLR bias in Fig. 1a. Active convection, with low OLR and high cloud cover, dominates at 5°N. The strongest events appear around the 4-7th, 14-16th and the 29-31st July in both the model and GERB data although OLR is most depressed in the model simulations.

The 4-7th event is also accompanied by an extension of the region of low OLR to the south in both the model and GERB data. The magnitude of OLR and cloud fraction anomalies are slightly underestimated by the model. Similar southward movement of cloud bands in the model around the 15th and over the period 18-24th July are not present in the satellite data leading to underestimates in model OLR by almost 100 Wm^{-2} at 5° S on the 20th. To investigate the cause of this discrepancy we consider 12 UTC data on the 5th and 19th July (marked as a thick horizontal line in Fig. 10a-b).

Figure 10c-d show maps of model and GERB OLR fields over the Gulf of Guinea (shading) for 12 UTC on the 5th July. Superimposed are contours of 500 mb vertical velocity (solid contours denote upward motion; dashed contours represent descent) from the model and NCEP reanalysis. The main area of convection over the Gulf of Guinea at 5° N is well captured by the model although a secondary convective system at 12°N is not present in the model. Upward vertical motion is present in both the NWP model and NCEP reanalysis along the 5-10° N latitude line. The region of depressed OLR ($<280 \text{ Wm}^{-2}$) running south from the main convective bands are well represented by the model, consistent with Fig. 10a-b. Analysing the EUMETSAT dust product, which uses the 12.0, 10.8 and 8.7 μm SEVIRI channels (not shown), the extensive area of low OLR corresponds with thick mid-level cloud rather than cirrus.

On the 19th July the model simulations contain bands of thick, high altitude clouds protruding across the equatorial Atlantic. This is not present in the GERB data, locally causing model underestimates in OLR approaching 100 Wm^{-2} . The model does capture the convective centres over and to the north west of the Gulf of Guinea and off the coast of Sierra Leone. It is not immediately clear why the model accurately simulates the extensive high altitude cloud on the 5th but not on the 19th. Comparing the vertical velocity fields there is some evidence to suggest that the convective region is less extensive on the 19th compared with the 5th for the NCEP data while the model vertical motion fields are consistent between the two dates. Also the NCEP data indicate a much larger region of

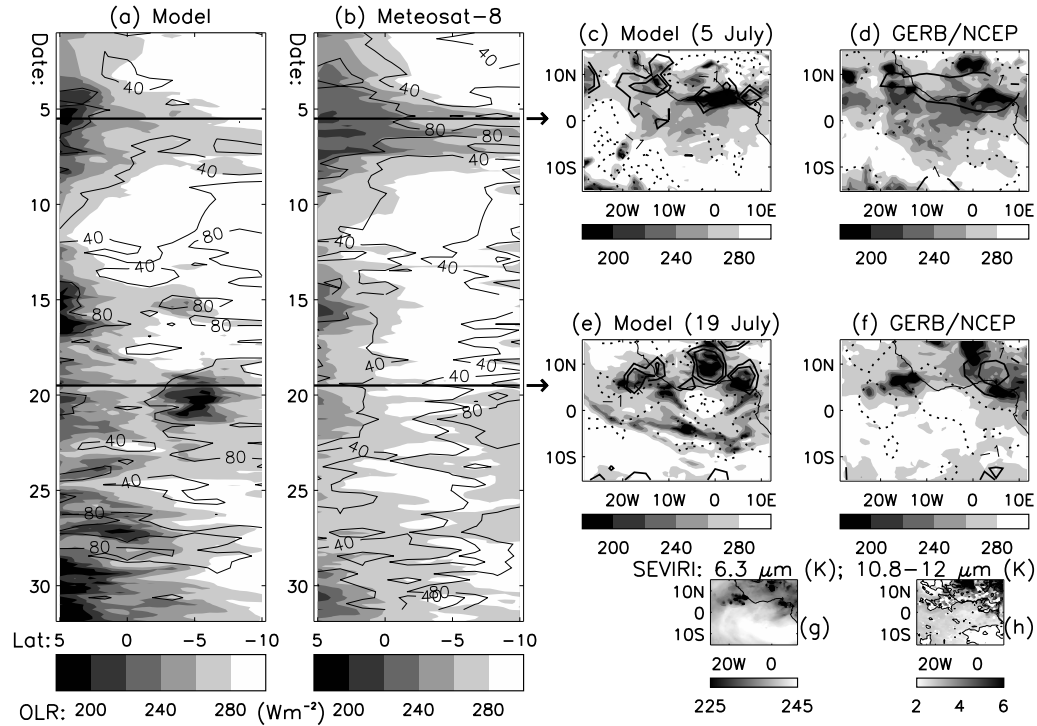


Figure 10. Time-latitude evolution of OLR (shading) and cloud fraction (contours) for (a) model and (b) GERB/MPEF during July 2006 using coincident 3-hourly data over the region 10°W - 5°E , 10°S - 5°N . Spatial OLR maps are shown for the model and GERB for the 5th July (c-d) and 19th July (e-f), marked as horizontal lines in a and b. Also shown in c-f are contours of vertical motion: solid denotes upward velocities (1 and 3 cm s^{-1}) while dashed contours denote downward motion (-1 and -3 cm s^{-1}). SEVIRI brightness temperature at (g) $6.3 \mu\text{m}$ and (h) the $10.8\text{-}12 \mu\text{m}$ difference are also shown for the 19 July; the MPEF 80% cloud fraction contour is overlaid in (h).

strong subsidence to the south west of the Gulf of Guinea on the 19th which may act to reduce humidity thereby dissipating cirrus cloud.

Another possibility is that cirrus cloud is present in the GERB data but is optically very thin. To test this hypothesis, brightness temperatures (BT) from SEVIRI channels are displayed in Fig. 10g-h. The $6.3 \mu\text{m}$ BT, sensitive to high altitude cloud and mid to upper tropospheric relative humidity (e.g. Brogniez *et al.* 2006), highlights the three main convective centres (BT $\sim 225 \text{ K}$) present in the GERB OLR field. Much of the ocean region to the south of the African coast experienced high BT ($\sim 245 \text{ K}$), symptomatic of a dry, cloud-free upper troposphere. The 10.8 minus $12 \mu\text{m}$ BT difference is sensitive to mineral dust aerosol (negative BT difference) and to thin cirrus cloud (BT difference greater than 5 K) (e.g., Luo *et al.* 2002). This shows positive differences of $\sim 5 \text{ K}$ over continental Africa, likely coinciding with cirrus cloud, but BT differences over the ocean are generally around 2 K suggesting that thin cirrus is not present. Overlaid in Fig. 10h is the 80% contour of MPEF cloud; this highlights the main convective centres as well as an area of marine stratocumulus cloud to the southeast of the region.

(d) *Marine Stratocumulus in the South Atlantic*

The effect of low-level stratiform clouds on the top of atmosphere radiation budget is large since they readily reflect sunlight whilst exerting only a marginal effect on the longwave radiative cooling to space. The net radiative cooling effect of these clouds is particularly large at local noon when the insolation is maximum and over ocean surfaces since the cloud reflectivity (or albedo) is much larger than the ocean surface. Whilst it is therefore important to simulate marine stratiform or stratocumulus clouds in models, this is by no means trivial. Marine stratus tends to form beneath the sub-tropical dry, descending branches of the Hadley circulation over cold ocean currents, generally to the west of continents (e.g. Klein and Hartmann 1993): these conditions favour subsidence which limits the growth of cumulus convection and maintains a moist boundary layer. Therefore the representation of stratocumulus cloud in models is highly sensitive to detailed structure in the boundary layer and the interaction between the boundary layer and convection schemes.

Considering 12 UTC data over the period April-September 2006 the largest positive model minus GERB bias in reflected shortwave radiation of around 60 Wm^{-2} occurs over the sub-tropical Atlantic ocean (Fig. 1c), coinciding with the primary marine stratocumulus belts. This is consistent with previous findings by Allan *et al.* (2006) who used preliminary GERB data to show that a previous version of the NWP model underestimated the reflectivity of marine stratocumulus cloud. In this section we extend the analysis by comparing the current version of the NWP model with Edition 1 GERB data. This is particularly important since updates to the physical parametrizations were implemented (Section 2); the time series of shortwave albedo differences over the global oceans (Fig. 2) suggest the removal of negative model minus GERB albedo in March 2006, coinciding with changes in the boundary layer scheme. The primary aims are therefore to assess (i) the variations in model bias over time, (ii) whether errors in cloud amount or reflectivity can explain the model bias and (iii) the effect of model changes on the simulation of stratocumulus over the period.

(i) *Spatial Structure*

Figure 11 shows the model and GERB shortwave albedo at 12 UTC over the south Atlantic stratocumulus region for the 5th June 2006. Consistent with previous comparisons (Allan *et al.* 2005) the model cloud coverage exhibits a curious banded structure, thought to relate to an unrealistic representation of the rising cloud top altitude with increasing boundary layer depth to the west, possibly due to inadequate vertical resolution (Lock *et al.* 2001).

• (## POSSIBLE FIGURE? - model level-longitude cross section of cloud fraction 5th June 2006 12 UTC?##) Sean/Malcolm

Also consistent with previous analysis over the period 2003-2005 (Allan *et al.* 2006), the cloudy region appears brighter in the model than the GERB data. We now assess in detail the radiative properties of low-level cloud in the region illustrated in Fig. 11.

(ii) *Cloud radiative composites*

To identify low-level stratiform cloud a method is adopted that allows consistent sub-sampling of the GERB and model data. To achieve this we use top of atmosphere radiative fluxes and cloud fraction available from the Meteosat-8 satellite and simulated by the NWP model. Marine stratocumulus cloud is

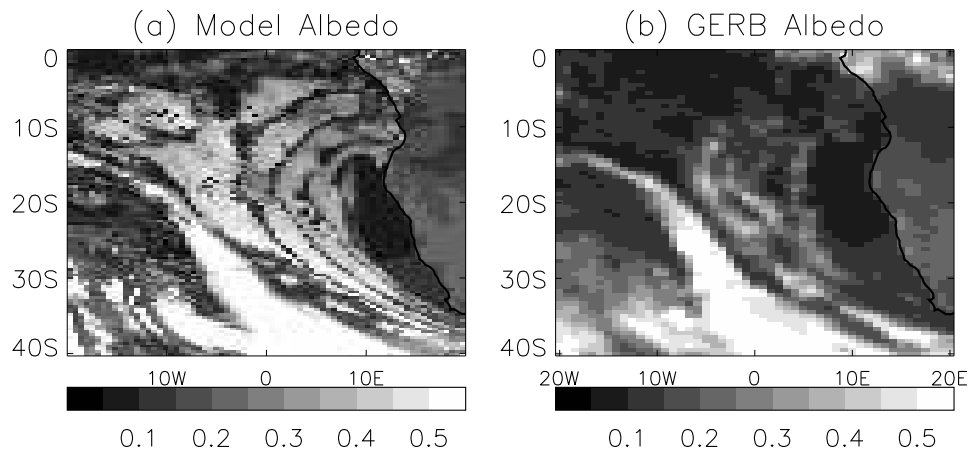


Figure 11. Shortwave albedo at 12 UTC, 5th June 2006 over the south-eastern sub-tropical Atlantic for (a) model and (b) GERB

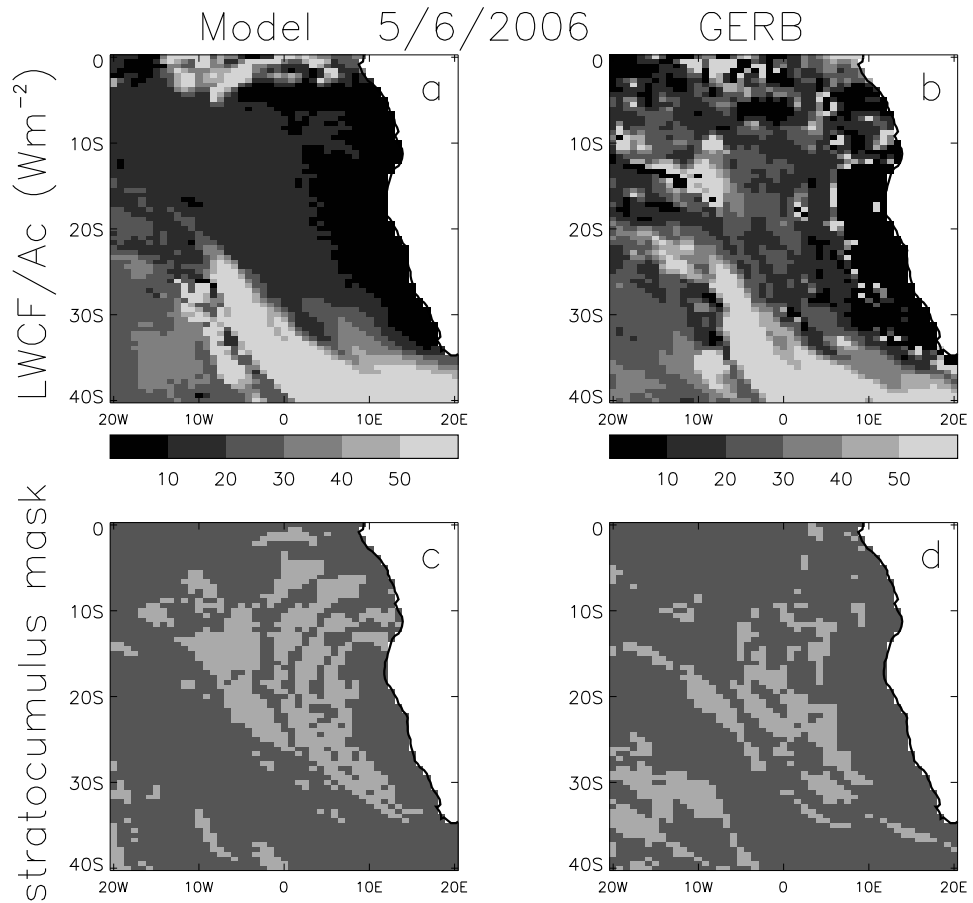


Figure 12. Illustration of marine stratocumulus identification for 12 UTC, 5 June 2006: LWCF normalised by cloud fraction for (a) model and (b) GERB and the stratocumulus mask (light shading) for (c) model and (d) GERB.

identified as follows:

$$\frac{LWCF}{Ac} \leq 30Wm^{-2}, \quad (6)$$

$$Ac > 0.8. \quad (7)$$

These criteria ensure the removal of higher altitude cloud and low-level broken cloud cover thereby concentrating on overcast low-altitude cloud scenes in the model and GERB data. The criteria in (6) is qualitatively consistent with a recent study by Futyan *et al.* (2005) who used EUMETSAT cloud classification (CLA) to estimate the Meteosat-estimated SWCF and LWCF contribution from high, medium and low cloud. In their Figure 1 (right panels) they find $LWCF < 20Wm^{-2}$ with a maximum cloud cover of 75% over the Namibian stratocumulus region.

While the identified scenes may contain various types of low-altitude cloud cover, for convenience we term the identified scenes as marine stratocumulus. It is also possible that contamination by thin cirrus may occur; it is expected that the dominant type of cloud identified will however be stratocumulus as illustrated by Futyan *et al.* (2005) for June 2004 over the south Atlantic.

Fig. 12a-b shows an example of the $LWCF/Ac$ parameter used in Eq. 6 for the same time as Fig. 11. If $Ac = 0$, $LWCF/Ac$ is also set to zero. Values over $30 Wm^{-2}$ are identified as high cloud: for example the bright stripe of cloud running from $20^{\circ}S, 10^{\circ}W$ to $40^{\circ}S, 0-10^{\circ}E$. The stratocumulus mask, determined by applying Equations 6-7, is shown in Fig. 12c-d. For this example, the model stratocumulus is generally more extensive than for the satellite data although more stratiform cloud is identified in the south west of the region for the satellite data.

Variations in cloud cover are presented in Fig. 13 using the 12 UTC data from April-September 2006. To improve interpretation, a 3-day moving average is applied to the data. The seasonal progression of the mean sea surface temperature (SST) is evident with maximum in April and minimum in September Fig. 13a. Coinciding with the reducing SSTs is a general increase in cloud fraction in both the model and satellite data (Fig. 13b), although the model increases are weaker leading to a slight underestimate in cloud fraction in the second half of the period considered.

Using Eq.(6) to remove high cloud events results in the time series displayed in Fig. 13c. This suggests that low-cloud changes explain most of the total cloud cover changes; diagnosed high cloud cover is generally stable at about 10-30% in the model and Meteosat data. Applying Equations 6-7, the resulting diagnosed variability of marine stratocumulus (Fig. 13d) suggests that much of the variability in cloud fraction results from changes in stratocumulus cloud cover. The model captures well the weekly fluctuations and monthly trend in stratocumulus cloud fraction although underestimates the cloud cover during August.

The calculated cloud albedo effect (ALBCF) for the diagnosed stratocumulus cloud cover region is presented in Fig. 13e. Only grid-points where both the model and observations indicate stratocumulus cloud cover are considered. This shows a systematic overestimation in stratocumulus cloud albedo, consistent with the mean comparisons in Fig. 1. However, the differences become smaller from July 2006 (## WHY IS THIS??).

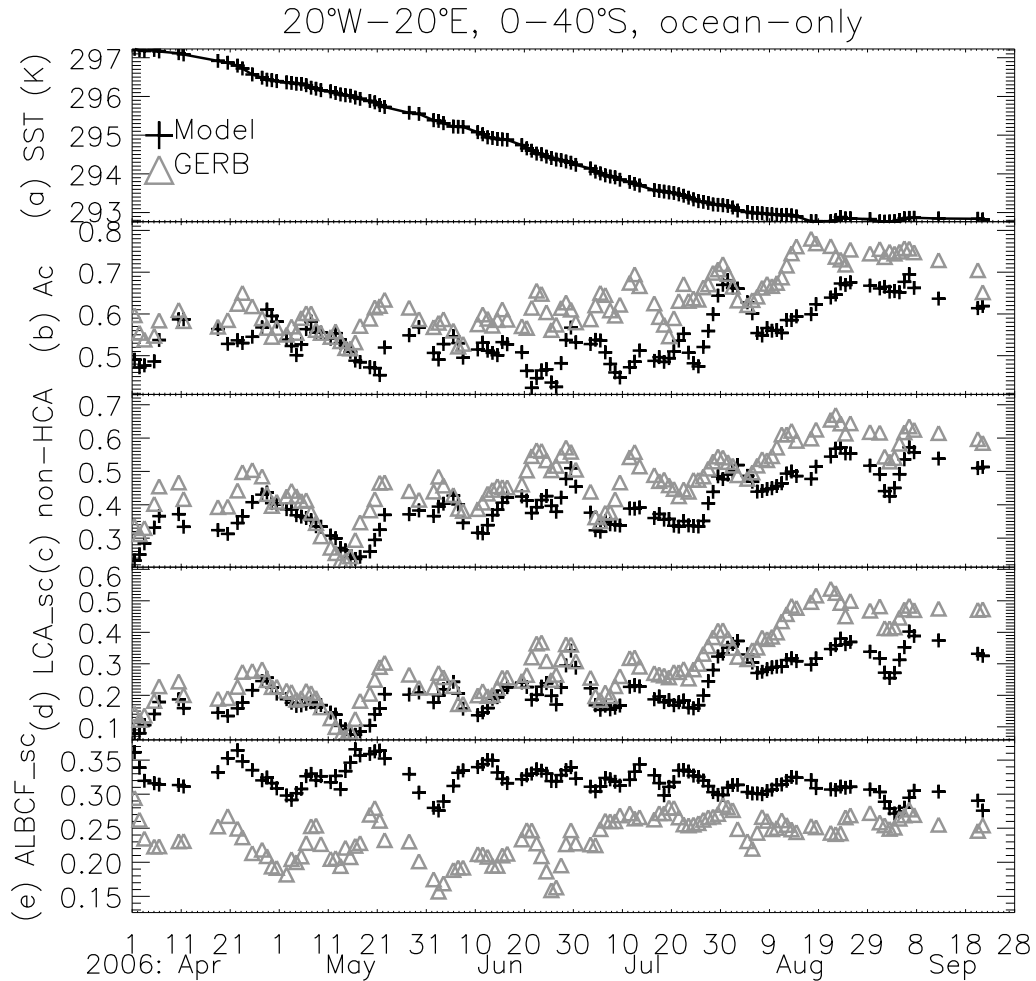


Figure 13. Time series of (a) SST, (b) cloud fraction, (c) non-high cloud fraction, (d) stratocumulus fraction and (e) stratocumulus cloud albedo effect at 12 UTC for the model and GERB/SEVIRI for April-September 2006.

To analyse the spatial nature of biases in stratocumulus properties, composites are formed based only on ocean grid points in which both the model and observations indicate stratocumulus cloud cover, using the criteria of Equations 6-7. A mean for the period April to September 2006 is calculated, removing grid points where coincident stratocumulus cover is not indicated more than 5% of the time. Fig. 14 shows the resulting composites for LWCF and ALBCF and also the frequency of occurrence of stratocumulus cloud cover in the model and GERB.

Figure. 14a-b shows a slightly lower magnitude of longwave cloud radiative effect in the model compared to GERB, although this is within the expected model clear-sky OLR error (Allan *et al.* 2005) which is used to construct both the model and GERB LWCF estimates. The increase in LWCF from east to west, in both the model and GERB, signifies an increase in cloud top altitude with increased SST and boundary layer height. However, while this progression is

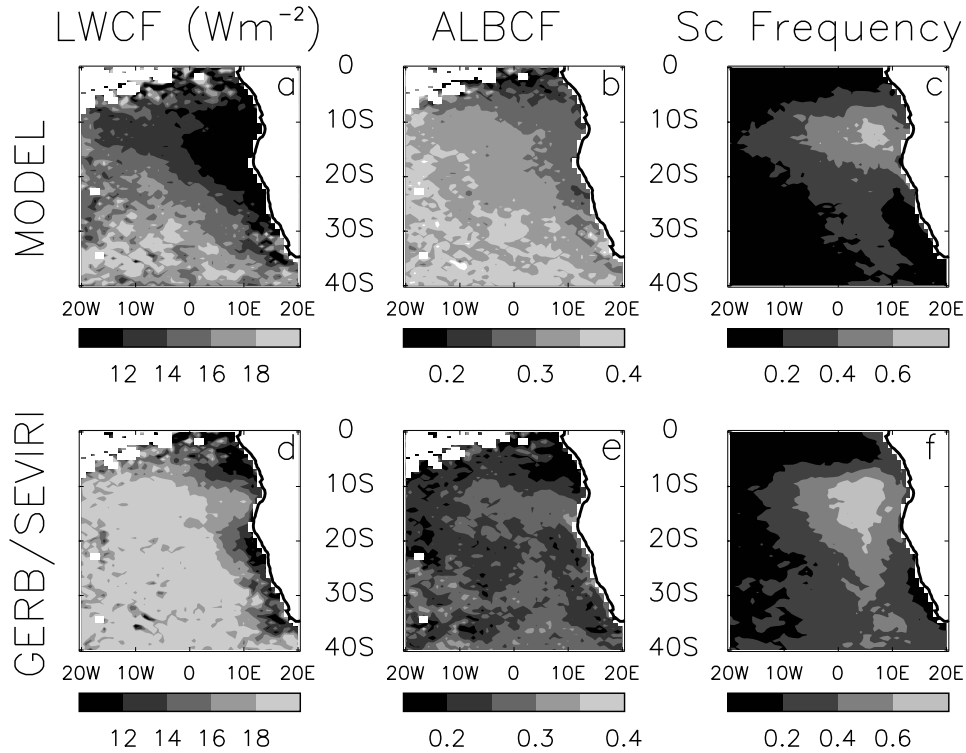


Figure 14. Model (a-c) and GERB/SEVIRI (d-f) composites of LWCF and cloud albedo effect (ALBCF) for pixels identified as stratocumulus and the frequency of stratocumulus identification for 12 UTC data over the period April-September 2006.

aligned east to west in the GERB data, it appears more north-east to south-west in the model.

A spatially similar increase in cloud albedo effect is present in the model suggesting a thickening of the cloud with increased boundary layer depth. This effect is not apparent in the GERB data which shows cloud albedo effect to remain fairly constant at around 0.25. Consistent with the time-series and mean comparisons, the model cloud albedo effect is substantially larger than found in the GERB data, ranging from 0.25 on the coast of Angola to 0.35 to the south west of the region considered. The frequency of occurrence of stratocumulus cloud in the model is similar but slightly lower than the Meteosat data (Fig. 14e-f). This suggests that the positive model bias in RSW shown in Fig. 1 is caused by an overestimation in stratocumulus cloud reflectivity rather than cloud fraction.

One possible explanation for the model bias in stratocumulus reflectivity is an overestimation of cloud liquid water (CLW). Considering June and July 2006, the model simulates a peak in CLW of nearly 0.1 mm for the primary stratocumulus region around 10° (Fig. 15). This peak is also apparent in the SSM/I data for July (Fig. 15e) but is not discernible for June (Fig. 15b). Errors in CLW for the north-east of the region considered are close to zero for July (Fig. 15f) but are overestimated by up to 0.04 mm by the model during June 2006 (Fig. 15c). The reduction in CLW bias from June to July coincides with a drop in the model overestimate in cloud albedo effect during this period (Fig. 13) suggesting that

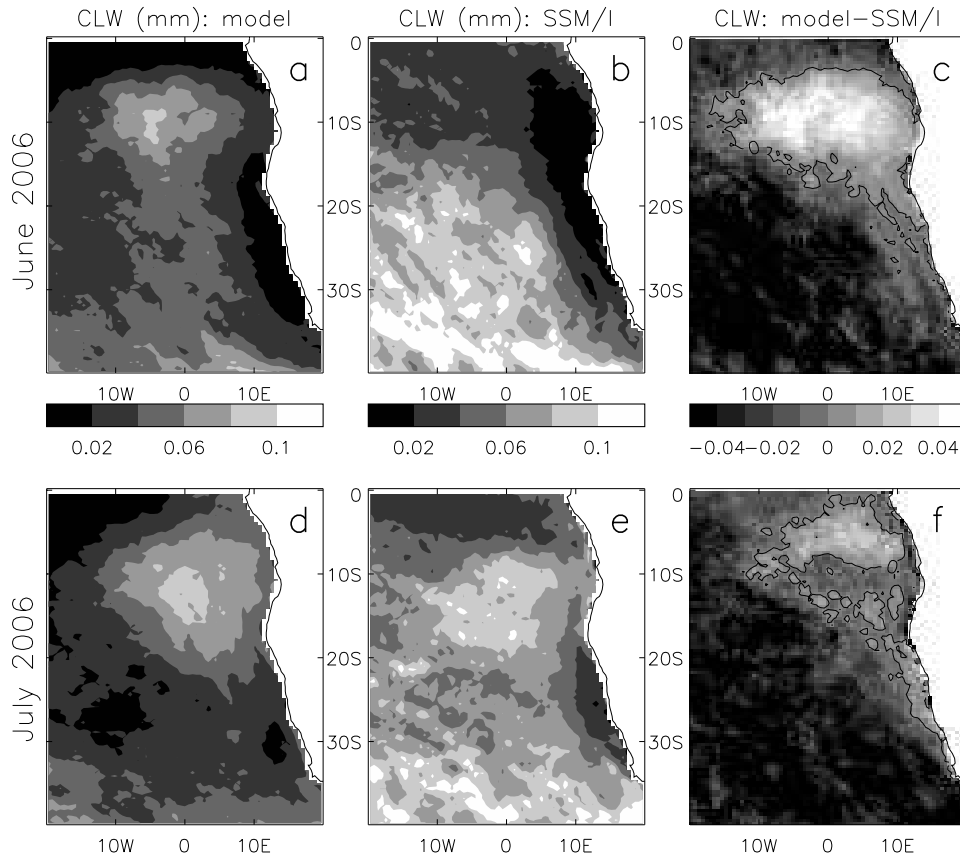


Figure 15. Monthly mean cloud liquid water (mm) from SSM/I, model and model minus SSM/I (including a contour at zero) for June (a-c) and July (d-f) 2006

the model bias in cloud reflectivity over the period April-June 2006 indeed relates to an overestimate in CLW.

For both June and July, the model CLW is lower than the SSM/I values for the south western portion of the region (Fig. 15). Over the global, ice-free oceans, CLW is underestimated by a factor of 2 compared to SSM/I data (not shown); this is most pronounced across tropical oceans, close to the ITCZ and South Pacific Convergence Zone. It is not clear why this is the case and the discrepancy merits further investigation. It is likely that the model CLW bias over stratocumulus regions can partly explain the bias in RSW compared to GERB data shown in Fig. 1c. It is also possible that the plane-parallel approximation for low-level stratiform cloud is unrealistic, contributing to the overestimation in simulated cloud reflectivity.

(iii) *Diurnal variability*

The cloud mask used in the previous sections is based upon shortwave radiance channel data and so is available only during daylight hours. Therefore to evaluate the diurnal variations of stratocumulus cloud an alternative product is used which samples throughout the diurnal cycle. The SEVIRI-based Meteorological Product Extraction Facility (MPEF) cloud mask (Schmetz *et al.* 2002) is

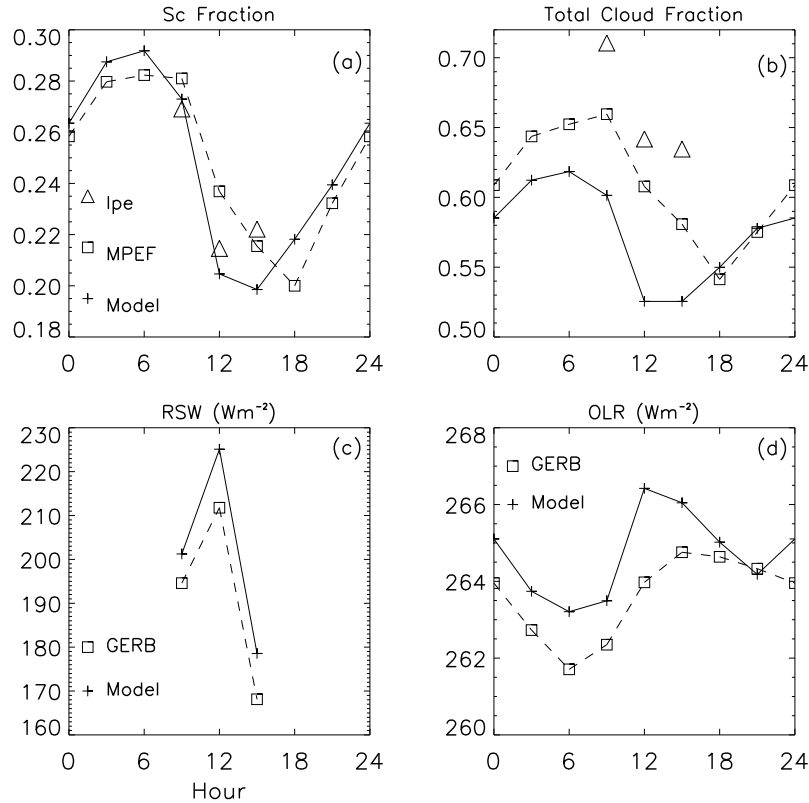


Figure 16. Mean diurnal cycle of (a) stratocumulus fraction, (b) total cloud fraction, (c) RSW and (d) OLR using coincident 3-hourly model and GERB/SEVIRI data for July 2006.

employed at a frequency of 3 hours during July 2006. To identify stratocumulus-type cloud we use the GERB-derived LWCF criteria developed in Section (d).

Figure 16a shows the observed diurnal variation in diagnosed stratocumulus is well captured by the model. There is a maximum stratocumulus cover at 06 UTC while minima occur at 15 UTC in the model and 18 UTC in the MPEF data. Also shown is the stratocumulus fraction calculated for the Ipe *et al.* (2004) shortwave cloud mask at 09, 12 and 15 UTC used in the previous section; this shows a minimum at 12 UTC illustrating that the observed diurnal cycle is sensitive to the cloud mask employed.

The total cloud fraction also displays a diurnal cycle (Fig. 16b) that is of similar magnitude to, and therefore resulting from, the stratocumulus cloud variation. The total cloud fraction is more than twice the stratocumulus fraction, with low-level trade cumulus and higher altitude cloud contributing to the total coverage. Both the MPEF and RMIB shortwave cloud fraction are greater than the model fraction by 5-10% throughout the day apart from the evening. Despite the model underestimate in cloud fraction, the simulated RSW is greater than the GERB values during the day by around $5-10 Wm^{-2}$. This is consistent with the model stratocumulus cloud being too reflective although the magnitude of the bias is small compared to the model minus GERB differences for the April-September period at 12 UTC displayed in Fig 1. The time-series in Fig. 13e suggests that this bias is influenced more by the period April-June while differences in

stratocumulus cloud reflectivity between the model and GERB are smaller in July-September. Both model and GERB data indicate that the higher amounts of stratocumulus at 09 UTC compared with 15 UTC contribute to the higher RSW in the morning ($\sim 200 \text{ Wm}^{-2}$) compared with the evening ($\sim 180 \text{ Wm}^{-2}$).

The diurnal cycle of OLR (Fig. 16d) corresponds well with the variation in cloud fraction which in turn is primarily due to changes in stratocumulus. Thus, despite the low-altitude cloud top heights, changes in stratocumulus exert a detectable influence on the OLR, although this variation is only of magnitude $\sim 3 \text{ Wm}^{-2}$. Similar results were found by Comer *et al.* (2007) using principle component analysis. The overestimate in model OLR by about 2 Wm^{-2} is consistent with a lower non-stratocumulus fraction in the model; these differences are within the expected uncertainty of the GERB data (Harries *et al.* 2005).

5. CONCLUSIONS

The Met Office global NWP model is evaluated using new data from the Geostationary Earth Radiation Budget (GERB) instrument on-board the Meteosat-8 satellite. Systematic differences between the model and GERB, larger than the expected uncertainty in the satellite data, are identified over the period April-September 2006.

- A model overestimate in shortwave albedo over the subtropical Atlantic ocean corresponds with areas of marine stratocumulus. The discrepancy is greatest for the period April-June and is consistent with a model overestimate in stratocumulus cloud liquid water content compared with SSM/I data in June which diminishes by July. An overestimate in LWC by the model over the main stratocumulus bands is likely to explain in part unrealistic radiative properties of marine stratocumulus. However, substantial underestimation in LWC by the model away from the main stratocumulus decks suggests that further analysis is required.

- A model underestimate in shortwave albedo over equatorial Africa relates to unrealistic radiative properties of deep convective cloud. The bias is sensitive to the convective parametrization and diminishes following the adoption of a convection decay time-scale within the model physics in December 2006.

- Unrealistic detrainment of convectively generated southward propagating cloud bands over the Gulf of Guinea are identified during July 2006, leading to local underestimation in OLR by up to 100 Wm^{-2} .

- An overestimation in model OLR over the Sahara of up to 40 Wm^{-2} is spatially correlated with high aerosol optical depth, consistent with previous analysis (Haywood *et al.* 2005).

- Despite and increase in model surface albedo to more realistic levels in January 2005 (Milton *et al.* 2005), there remain errors in the spatial structure of surface albedo based on comparisons of clear-sky top of atmosphere albedo. The model underestimates clear-sky RSW by up to 100 Wm^{-2} at 1200 UTC over the Sahel and northern coastal regions of Africa.

- A model overestimate in OLR and underestimate in RSW at 1200 UTC over Europe is symptomatic of unrealistically low cloud radiative effect.

The combination of GERB data with additional information from other satellite instruments and reanalysis datasets provide a powerful tool for examining the causes of errors in the NWP model and for aiding the development of new

parametrizations. The methodology described will be continued, extending the current analysis period, as more release version GERB data becomes available.

ACKNOWLEDGEMENTS

Thanks to the GERB International Science Team. The GERB and SEVIRI data were taken from the GGSPS and RMIB archives; the SSM/I data from www.ssmi.com; the MISR data were extracted from the NASA Langley DAAC and the NCEP/NCAR reanalysis data from the NOAA Earth Systems Research Laboratory (www.cdc.noaa.gov). This work was funded under NERC contracts NER/D/S/2002/00412 and NE/C51785X/1.

REFERENCES

- Allan, R. P., Slingo, A., Milton, S. F. and Culverwell, I. 2005 Exploitation of geostationary Earth radiation budget data using simulations from a numerical weather prediction model: Methodology and data validation. *J. Geophys. Res.*, **110**, D14111, doi:10.1029/2004JD005698
- Allan, R. P., Slingo, A., Milton, S. F. and Brooks, M. E. 2006 'Exploitation of geostationary Earth Radiation Budget (GERB) data from 2003-2006 in the evaluation of the Met Office global NWP model'. Pp. XX-XX in Proceedings of the EUMETSAT Meteorological Satellites Conference, 12-16 June 2006, Helsinki, Finland, EUMETSAT, Darmstadt, Germany. *in press*
- Brogniez, H., Roca, R. and Picon, L. 2006 A clear-sky radiance archive from Meteosat "water vapor" observations. *J. Geophys. Res.*, **111**, D21109 doi:10.1029/2006JD007238
- Comer, R. E., Slingo, A. and Allan, R. P. 2007 Observations of the diurnal cycle of outgoing longwave radiation from the Geostationary Earth Radiation Budget instrument. *Geophys. Res. Lett.*, **under review**
- Diner, D. J., Abdou, W. J., Conel, J. E., Crean, K. A., Gaitley, B. J., Helmlinger, M., Kahn, R. A., Martonchik, J., V. and Pilorz, S. H. 2001 MISR aerosol retrievals over southern Africa during the SAFARI-2000 dry season campaign. *Geophys. Res. Lett.*, **28**, 3127-3130
- Futyan, J. M., Russell, J. E. and Harries, J. M. 2005 Determining cloud forcing by cloud type from geostationary satellite data. *Geophys. Res. Lett.*, **32**, L08807, doi:10.1029/2004GL022275
- Harries, J. E. and 44 coauthors 2005 The Geostationary Earth Radiation Budget project. *Bull. American Meteorol. Soc.*, **86**, 945-960
- Haywood, J. M., Allan, R. P., Culverwell, I., Slingo, A., Milton, S., Edwards, J. and Clerbaux, N. 2005 Can desert dust explain the outgoing longwave radiation anomaly over the Sahara during July 2003? *J. Geophys. Res.*, **110**, D05105, doi:10.1029/2004JD005232
- Ipe, A., Clerbaux, N., Bertrand, C., Dewitte, S. and Gonzalez, L. 2004 Validation and homogenisation of cloud optical depth and cloud fraction retrievals from GERB/SEVIRI scene identification using Meteosat-7 data. *Atmos. Res.*, **72**, 17-37, doi:10.1016/j.atmosres.2004.03/010
- Kalnay, E. M., et al. 1996 The NCEP/NCAR 40-year reanalysis project. *Bull. Am. Meteorol. Soc.*, **77**, 437-471
- Klein, S. A. and Hartmann, D. L. 1993 The seasonal cycle of low stratiform clouds. *J. Climate*, **6**, 1587-1606
- Lock, A. P. 2001 The numerical representation of entrainment in parameterizations of boundary layer turbulent mixing. *Mon. Wea. Rev.*, **129**, 1148-1163
- Luo, Z., Rossow, W. B., Inoue, T. and Stubenrauch, C. J. 2002 Did the eruption of the Mt. Pinatubo volcano affect cirrus properties. *J. Climate*, **15**, 2806-2820

- Milton, S. F., Brooks, M., Lock, A., Whelan, E., Wilson, D. and Allan, R. 2005 'HadGEM1 Physics for the Global NWP Model (Cycle G34): Improvements to Boundary Layer, Large Scale Precipitation, Convection and Saharan Albedo'. Pp. 39, *NWP Technical report 458*, Met Office, UK
- Schmetz, J., Pili, P., Tjemkes, S., Just, D., Kerkmann, J., Rota, S. and Ratier, A. 2002 An Introduction to Meteosat Second Generation (MSG). *Bull. Amer. Meteorol. Soc.*, **83**, 977–992
- Slingo, A., Ackerman, T. P., Allan, R. P., Kassianov, E. I., McFarlane, S. A., Robinson, G. J., Barnard, J. C., Miller, M. A., Harries, J. E., Russell, J. E. and Dewitte, S. 2006 Observations of the impact of a major Saharan dust storm on the Earth's radiation balance. *Geophys. Res. Lett.*, **in press**
- Slingo, A., Hodges, K. I. and Robinson, G. R. 2004 Simulation of the diurnal cycle in a climate model and its evaluation using data from Meteosat 7. *Q. J. R. Meteorol. Soc.*, **130**, 1449–1467
- Trenberth, K. E. and Guillemot, C. J. 1998 Evaluation of the atmospheric moisture and hydrological cycle in the NCEP/NCAR reanalysis. *Clim. Dyn.*, **14**, 213–231
- Wentz, F. J. 1997 A well-calibrated ocean algorithm for SSM/I. *J. Geophys. Res.*, **102**, 8703–8718